Oxidized Polysaccharides for Anticancer-Drug Delivery: What is the Role of Structure?

Lukáš Münster,[1] Michaela Fojtů,[2,3] Zdenka Capáková,[1] Monika Muchová, [1] Lenka Musilová, [1] Tomáš Vaculovič,[4] Jan Balvan[2,5], Ivo Kuřitka,[1] Michal Masařík,[2,3,5,6] Jan Vícha [1*]*

[1]Centre of Polymer Systems, Tomas Bata University in Zlín, tř. Tomáše Bati 5678, 760 01 Zlín, Czech Republic

[2]Department of Physiology, Faculty of Medicine, Masaryk University, Kamenice 5, CZ-625 00 Brno, Czech Republic

[3]Center for Advanced Functional Nanorobots, Department of Inorganic Chemistry, Faculty of Chemical Technology, University of Chemistry and Technology in Prague, Technická 5, Prague CZ-166 28, Czech Republic

[4]Department of Chemistry, Faculty of Science, Masaryk University, Kamenice 5, CZ-625 00 Brno, Czech Republic

[5]Department of Pathological Physiology, Faculty of Medicine, Masaryk University, Kamenice 5, CZ-625 00 Brno, Czech Republic

[6]BIOCEV, First Faculty of Medicine, Charles University, Průmyslová 595, 252 50, Vestec, Czech Republic

Emails: jvicha@utb.cz, masarik@med.muni.cz

Abstract:

Study provides an in-depth analysis of the structure-function relationship of polysaccharide anticancer drug carriers and points out benefits and potential drawbacks of differences in polysaccharide glycosidic bonding, branching and drug binding mode of the carriers. Cellulose, dextrin, dextran and hyaluronic acid have been regioselectively oxidized to respective dicarboxylated derivatives, allowing them to directly conjugate cisplatin, while preserving their major structural features intact. The structure of source polysaccharide has crucial impact on conjugation effectiveness, carrier capacity, drug release rates, *in vitro* cytotoxicity and cellular uptake. For example, while branched structure of dextrin-based carrier partially counter the undesirable initial burst release, it also attenuates the cellular uptake and the cytotoxicity of carried drug. Linear polysaccharides containing β-(1→4) glycosidic bonds and oxidized at C2 and C3 (cellulose and hyaluronate) have the best overall combination of structural features for improved drug delivery applications including potentiation of the cisplatin efficacy towards malignances.

Keywords: drug delivery; cellulose; dextran; dextrin; sodium hyaluronate; selective oxidation;

1. Introduction

Platinum anticancer complexes such as cisplatin (CP), *cis*-[$Pt(NH_3)_2Cl_2$], represent a first-line therapy in the treatment of patients diagnosed with lung, ovarian, cervix, bladder, testicular, or head and neck cancer. The treatment is however complicated by severe side effects including nausea, neurotoxicity, nephrotoxicity, and ototoxicity due to cumulative toxicity and non-specific mechanisms of action of platinum anticancer drugs. (Raudenska et al., 2019) Various strategies aiming to reduce their severe side effects were employed over the past years. (Johnstone et al., 2016) Conjugation of platinum-based cytostatics to macromolecular carriers is among the most successful ones because it reduces their toxicity, prolongs circulation time in blood and introduces a passive accumulation of the drug in the tumor due to the enhanced permeability and retention (EPR) effect. (Wang & Guo, 2012)

Polysaccharides and their derivatives have been extensively investigated as anticancer-drug carriers due to their natural origin, biocompatibility and excellent potential for modifications. (Huang et al., 2015) They are, however, also notoriously known for their structural diversity, which may complicate - but hypothetically also enhance - their drug delivery capabilities. Yet, the data regarding the impact of structural features of polysaccharide-based carriers on the platinum drug delivery are often limited to investigating the role of single factor, typically the molecular weight of the polysaccharide (Varshosaz, 2012) or to the comparison of drug delivery performance of various derivatives of the same polysaccharide, see for instance (Schlechter et al., 1989; Ohya et al., 1996; Ohta et al., 2016). To obtain insight into the structure-function relationship of various polysaccharides, one usually has to rely on indirect comparison found in review articles (Goodarzi et al., 2013; Miao et al., 2018) because of the lack of studies directly and methodically comparing drug delivery characteristics of structurally diverse polysaccharides. This is not very surprising because most of the polysaccharides does not actually contain functional groups suitable for the direct binding of platinum complexes.

Regioselective oxidation of polysaccharides to corresponding dicarboxypolysaccharides (DCPs), (Khomyakov et al., 1965; Kristiansen et al., 2010; Sirviö et al., 2014) provides a unique opportunity to remedy this issue. Sequential periodate/chlorite oxidation introduces two –COOH groups per each oxidized unit, which can directly conjugate the majority of platinum(II) complexes, while preserving the main structural features of source polysaccharides intact. The only prerequisite is the presence of a pair of hydroxyl groups on neighboring carbon atoms (vicinal diol) in the polysaccharide structure.

In this work, direct and in-depth analysis of potential benefits and drawbacks of individual structural features of polysaccharide-based platinum-drug carriers has been performed in order to confirm our hypothesis about certain structural aspects having potential for improving their drug delivery characteristics. The two-stage oxidation of four structurally different polysaccharides (cellulose, dextrin, dextran and hyaluronic acid) was performed. Special attention was paid to their preparation and detailed structural characterization. Carriers differing in configuration of binding sites, drug binding effectiveness, type of the glycosidic bond(s), presence of branching and molecular weight were loaded with equivalent amount cisplatin and compared. The regioselectively oxidized dextrin and hyaluronic acid were, to the best of our knowledge, used as platinum drug carriers for the first time. The impact of each feature to cisplatin loading capacity and binding effectivity, release kinetics, *in vitro* cytotoxicity and cellular uptake has been investigated by combination of experiment and theory and is discussed in the manuscript. Besides pointing

out the effect of carrier's structural aspects, the results of this screening study will be used to identify the most promising carriers for future studies, including *in vivo* evaluation.

Structures of source polysaccharides and corresponding DCPs are given in Figure 1. Short description of selected polysaccharides summarizing their structural specifics and applications of their oxidized derivatives is given below.

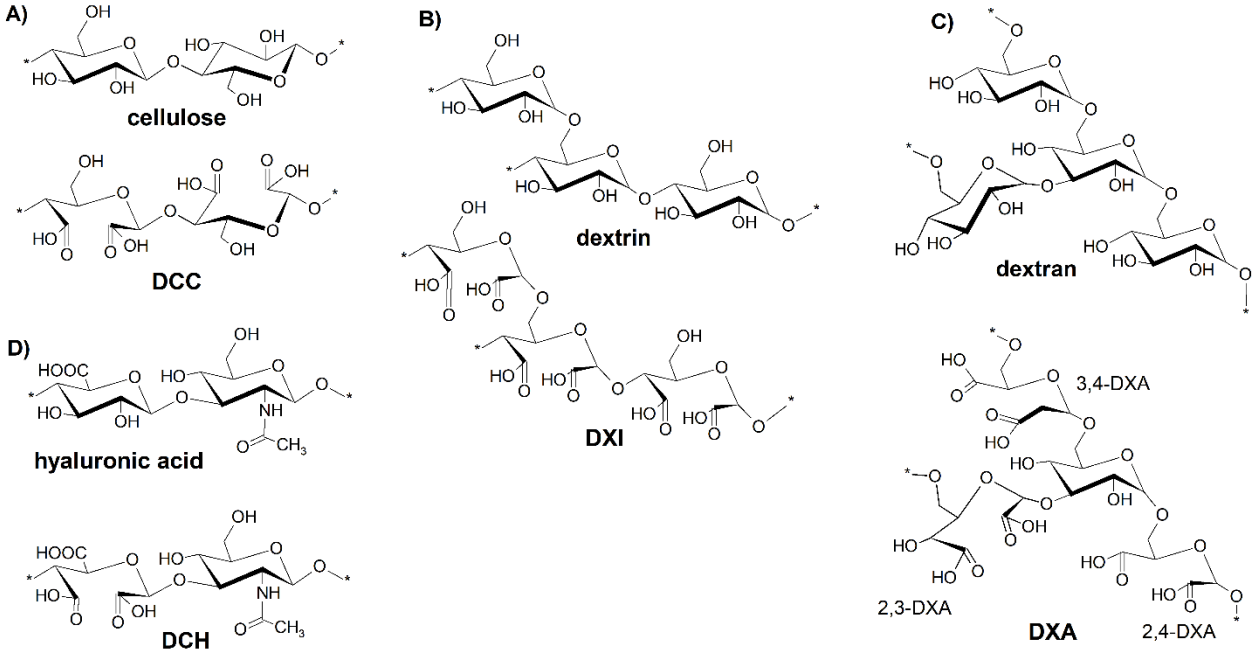

Figure 1 Structures of studied polysaccharides and their oxidized derivatives, A) cellulose/DCC, B) dextrin/DXI, C) dextran/DXA with non-oxidized, 2,3-, 3,4- and 2,4-oxidized units, D) hyaluronic acid/DCH.

Cellulose is the most abundant biopolymer worldwide and can be found in various plants, tunicates and bacteria. It is insoluble in water because its linear chains of anhydroglucose units (AGUs) joined by β-(1→4) glycosidic bonds tend to form crystalline structures densely bound by hydrogen bridge network. The preparation, properties and applications of selectively oxidized cellulose, 2,3-dicarboxycellulose (DCC in Figure 1A), are well studied. (Maekawa & Koshijima, 1984; Münster et al., 2019, 2020; Sirviö et al., 2014) DCC is capable of binding the CP with efficiency above 90% and it can carry over 50 wt% of CP while still retaining good aqueous solubility. (Münster et al., 2019) The cytotoxicity of CP-DCC conjugates can be modulated to the certain extent by controlling the molecular weight of the DCC during the synthesis. (Münster et al., 2020) In this work, DCC is used as a reference for comparison of other carriers due to its relatively simple structure and well understood chemistry and properties.

Dextrin is a product of hydrolysis of starch or glycogen. It has a branched structure due to the presence of α-(1→4) and α-(1→6) glycosidic bonds. It is partially or fully soluble in water, depending on its molecular weight. Drug delivery applications of dextrin derivatives are mostly limited to cyclodextrins, cyclic oligosaccharides featuring cavity with the hydrophobic inner surface, which are employed as carriers for hydrophobic species, (Babjaková et al., 2016) including platinum anticancer drugs. (Shi & Dabrowiak, 2012) Contrary, no applications of 2,3-dicarboxydextrin (DXI, Figure 1B) were found in available literature.

Comparison of DXI and DCC will allow to study the influence of the branched structure and the impact of α- vs. β- glycosidic bonds.

Dextrans are complex glucans of microbial origin composed of AGU chains bonded predominantly by α-(1→6) glycosidic bonds with α-(1→3) branching. They are produced by *Leuconostoc* and *Streptococcus* genus of bacteria and their structure and properties differ not only for different species of bacteria but also for different strains. (Sarwat et al., 2008) Drug-delivery applications of dextran and its derivatives are broad and summarized in several reviews. (Mehvar, 2000; Varshosaz, 2012) Periodate oxidation of dextran is no longer selective to positions 2 and 3 due to the presence of three neighboring hydroxyl groups at C2, C3 and C4, see Figure 1C. Dextran thus can be oxidized to 2,3-, 3,4- and 2,4-dialdehydedextran, respectively. (Khomyakov et al., 1965; Kristiansen et al., 2010) Secondary oxidation by chlorite then produces corresponding dicarboxydextrans (Khomyakov et al., 1965) (Figure 1C) collectively referred to as DXA in this work. In contrast, AGUs with α-(1→3) branching do not contain any vicinal hydroxyl groups and are thus entirely resistant to periodate oxidation. (Kristiansen et al., 2010) The DXA will be predominantly used to study the influence of the different (varied) composition of cisplatin binding sites.

Hyaluronic acid (HA) is an anionic glycosaminoglycan composed of D-glucuronic acid and N-acetyl-D-glucosamine bound by alternating β-(1→4) and β-(1→3) glycosidic bonds. HA is abundant in the human extracellular matrix, synovial fluid, cartilages, muscular connective tissues, skin and more. (Fraser et al., 1997) It is often employed for platinum anticancer-drug delivery, although it features only single –COOH group per basic structural unit, which limits maximum drug loading and binding effectiveness and may lead to undesirable crosslinking reactions influencing the solubility of drug-HA conjugate. (Cai et al., 2008; Fan et al., 2015) On the other side, HA binds to the CD44 receptor, an adhesion glycoprotein found on the surface of many cells, including malignant ones. CD44 is an integral component of the extracellular matrix involved in cell-cell and cell-matrix interactions. (Borland et al., 1998; Goodison et al., 1999) Expression of CD44 is increased in malignant tissue and may, therefore, serve as a diagnostic and prognostic marker (Assmann et al., 2001) or to target cancer cells and to increase the cellular uptake of drug-HA conjugates. (Quan et al., 2014)

Although the periodate oxidation of HA to 2,3-dialdehyde hyaluronate is commonly used modification *i.e.* for preparation of HA-based hydrogels, (Schanté et al., 2011) no mentions about 2,3-dicarboxyhyaluronate (DCH, Figure 1D) were found in available literature. This is rather quite remarkable, because two-stage selective oxidation essentially triples the amount of –COOH group in the molecule, which can be used not only to increase the carrier capacity but potentially also to open new pathways for the preparation of novel HA derivatives. Here, DCH is predominantly used to study the impact of different chemical composition of its units, biological targeting ability based on its affinity towards CD44 receptor and the lower density of carboxylic groups (only D-glucuronic acid units are susceptible to oxidation).

2. Materials and Methods

2.1 Materials. Cellulose SigmaCell type 20, Dextrin from corn starch type I, Dextran from *Leuconostoc spp.* (Sigma Aldrich Co.) and sodium hyaluronate from Contipro Ltd. (Czech Republic) were used as source polysaccharides. The weight-average molecular weight (M_w) of cellulose, dextrin, dextran and hyaluronic

acid were estimated by GPC analysis to be 76 kDa (degree of polymerization *DP* = 469, polydispersity index PDI = 4.7), 52 kDa (*DP* = 326, PDI = 2.3), 71 kDa (*DP* = 449, PDI = 1.8) and 329 kDa (*DP* = 820, PDI = 1.2), respectively. The chemicals employed in the primary oxidation of polysaccharide included sodium periodate ($NaIO_4$) and ethylene glycol (Penta, Czech Republic). Secondary oxidation of polysaccharides was performed using sodium chlorite ($NaClO_2$, 80%) in the presence of acetic acid (CH_3COOH, ≥99.8%) (both from Sigma Aldrich Co.), sodium acetate trihydrate ($CH_3COONa{\cdot}3H_2O$, Penta, Czech Republic) and sodium hydroxide (NaOH, Lachner, Czech Republic). Other chemicals involved in the characterization of DCPs included sodium nitrate ($NaNO_3$, Lachner, Czech Republic), disodium phosphate (Na_2HPO_4, VWR, Czech Republic), deuterium oxide (D_2O, Sigma Aldrich, Co.) and phosphate buffer saline (PBS, Invitrogen, USA). Reagents used for the biological experiments included fetal bovine serum (FBS) (mycoplasma-free), penicillin-streptomycin, trypsin, Dulbecco's Modified Eagle's Medium (DMEM) and and RPMI-1640 medium phosphate-buffered saline pH 7.2 (PBS), 3-(4,5-dimethylthiazol-2-yl)-2,5-diphenyl tetrazolium bromide (MTT) reagent, ethylenediaminetetraacetic acid (EDTA), dimethyl sulfoxide (DMSO), glycine buffer and hydroxyethyl-piperazineethane-sulfonic acid buffer (HEPES) (Merck, Germany). All chemicals were of analytical grade and were used without further purification. Demineralized water with the conductivity below 0.1 µS/cm was used throughout the experiments.

2.2 Preparation of 2,3-dicarboxypolysaccharides. The primary oxidation is started by dropwise addition of concentrated $NaIO_4$ solution to the suspension (cellulose, dextrin) or solution (dextran, hyaluronate) of 1 g of source polysaccharide in water. (Münster et al., 2017, 2018) Resulting concentration of $NaIO_4$ was 33 mg/mL for cellulose, dextrin and dextran (molar ratio of AGU : $NaIO_4$ was 1:1.25) and 16.5 mg/mL (molar ratio of AGU : $NaIO_4$ was 1:1.53) for HA to minimize its degradation. After the addition of $NaIO_4$, the reaction mixture was stirred at 30 °C in the absence of light. Individual reaction times were established based the UV/VIS spectral analysis of absorption band of periodate ion at 220 nm for 96 h, Figure 2. (Maekawa & Koshijima, 1984)

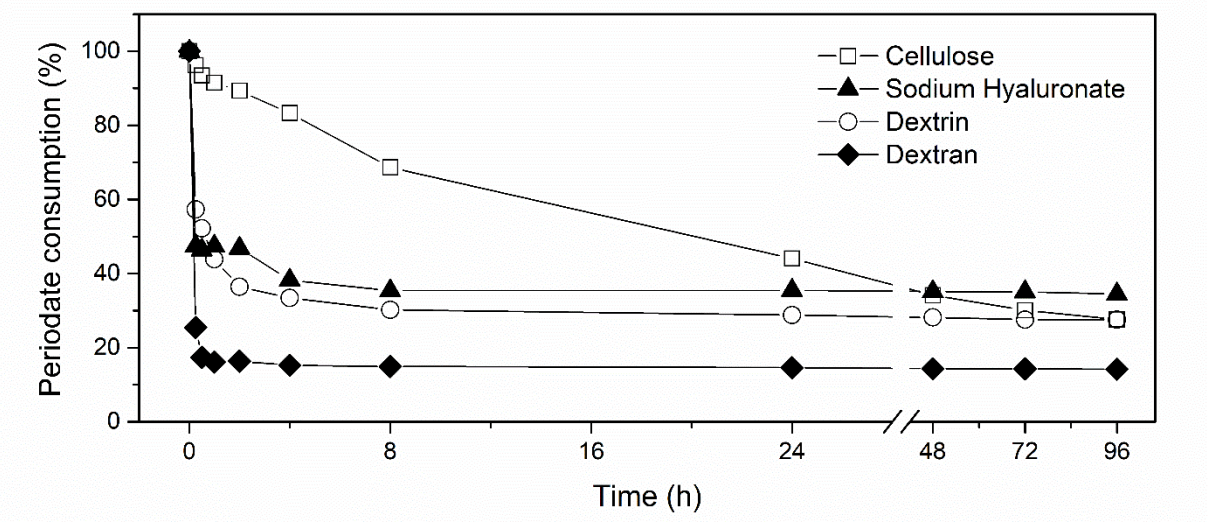

Figure 2 The periodate consumption during the primary oxidation of selected polysaccharides over 96 h.

As can be seen in Figure 2, the primary oxidation of cellulose, sodium hyaluronate, dextrin and dextran were largely completed after 72, 8, 8 and 4 h, respectively. However, because only D-glucuronic acid units

of HA are susceptible to oxidation and the density of oxidized group would thus be much lower than in case of other tested polysaccharides, it was decided to prolong the duration of primary oxidation of HA to 24 h in order to achieve the highest possible degree of oxidation (*DO)*. Subsequently, the oxidation reaction was terminated by the addition of excess ethylene glycol. Resulting dialdehyde polysaccharides were purified via suitable method, *i.e.* dialdehyde cellulose (DAC) was repeatedly centrifuged and mechanically homogenized using WiseTis homogenizer HD-15 (Witeg, Germany) and dialdehyde dextrin (DAXI), dialdehyde dextran (DAXA) and dialdehyde hyaluronate (DAH) were purified by dialysis against demineralized water for 48 h (14 kDa molecular weight cut-off, *MWCO*, Sigma Aldrich Co.). These purified products were then flash-frozen at -80 °C and lyophilized. The yields of the products of primary oxidation (relative to source polysaccharide) were 54.7 ± 0.6% for DAC, 84.6 ± 0.7% for DAXI, 94.6 ± 0.5% for DAXA and 98.8 ± 0.3% for DAH. Lower recovery of DAC is caused by material losses during repeated centrifugation and mechanical homogenization cycles used for purification.

Dialdehyde polysaccharides were subsequently oxidized by $NaClO_2$ (–CHO : $NaClO_2$ molar ratio 1:4, assuming 12.5 mmol/g of –CHO in DAC, DAXI and DAXA and 5.01 mmol/g of –CHO in DAH). (Münster et al., 2019, 2020) The concentration of $NaClO_2$ was set to 1 M for DAC and 0.5 M for other derivatives to limit their degradation based on previous findings. (Münster et al., 2020). The oxidation reactions of DAC, DAXI and DAXA were performed in the presence of 0.5 M CH_3COOH. Acetate buffer composed of 0.045M $CH_3COONa{\cdot}3H_2O$ and 0.055M acetic acid (pH 4.5) was used for DAH oxidation. The secondary oxidation started by the dropwise addition of concentrated $NaClO_2$ solution into the acidified solution of given dialdehyde and reaction ran for 7 h at 30 °C in the absence of light. (Münster et al., 2020) Reaction was terminated by addition of 10 M NaOH, products were purified by dialysis against demineralized water using *MWCO* = 14 kDa dialysis tubing. After the dialysis, the sample volume was reduced by rotary evaporator to approx. one quarter, pH set to 7.4 by 0.1 M NaOH, solutions filtered using 0.22 µm PTFE syringe filters, flash-frozen and lyophilized.

The degree of oxidation (*DO*) of prepared DCPs corresponds to percentage of basic structural units of given polysaccharide converted to dicarboxylated derivatives. It was determined from NMR spectra by comparison of signal intensities of oxidized and residual non-oxidized units, the latter being found mostly in region between 3.4 – 3.6 ppm, see (Münster et al., 2019, 2020) for more details.

2.3 UV/VIS and FT-IR spectral analysis. Double-beam UV/VIS spectrometer Lambda 1050 (PerkinElmer, USA) was utilized in a span of 180–800 nm for the analysis of the periodate consumption during the primary oxidation, employing measurements of aliquot samples collected in a timeframe ranging from 15 min to 96 h after the periodate oxidation initiation.

Qualitative FT-IR analysis (see Supplementary data) was performed on prepared DCPs and their conjugates with CP, using the infrared spectrometer Nicolet 6700 FT-IR (Thermo Fisher Scientific, USA) equipped with the ZnSe crystal in the ATR mode in a span of wavelengths 4000–700 cm^{-1} (res.: 4, scans: 64, the suppression of atmospheric gases enabled).

2.4 NMR, GPC and DLS analysis. All ^{1}H, ^{13}C and ^{1}H-^{13}C correlation spectra were measured using Bruker Avance III HD 700 MHz NMR spectrometer (Bruker, USA) equipped with a triple-resonance cryoprobe optimized for ^{13}C detection at 298 K in D_2O. The ^{1}H–^{13}C multiplicity-edited heteronuclear single quantum

correlation (HSQC, J_{H-C} = 145 Hz) and $^{1}H-^{13}C$ heteronuclear multiple bond correlation (HMBC, $^{n}J_{H-C}$ = 10 Hz) experiments were used based on the previous experience. (Münster et al., 2017)

Molecular weight distribution was analyzed by the gel permeation chromatography (GPC) using a Waters HPLC Breeze chromatographic system (Waters, USA) set up with a Waters 2414 refractive index detector (drift tube T = 60 °C), Tosoh TSK gel $GMPW_{XL}$ column (300 mm × 7.8 mm × 13 µm, column T = 30 °C). A mixture of 0.1 M $NaNO_3$ and 0.05 M Na_2HPO_4 was employed as a mobile phase. Calibration was carried out using pullulan polysaccharide calibration kit SAC-10 (Agilent Technologies, USA) in a span of M_w 342–805 000 g/mol.

Zeta potential (ζ) and hydrodynamic radii of conjugate nano-assemblies were determined in demineralized water and 0.15 M NaCl solution by dynamic light scattering (DLS) method using a Zetasizer Nano ZS90 instrument (Malvern Instruments, UK). The measurements were performed at 25 °C on a DTS1070 cell using the Smoluchowski model.

2.5 Preparation of cisplatin-carrier conjugates, loading and release study. CP was selected as a model drug because of its wide employment in clinical practice. It was prepared by using well-established procedures (Wilson & Lippard, 2014), dissolved in water (2 mg/mL) and added dropwise to the 4 mg/mL aqueous solution of the carrier at room temperature. It was gently shaken for 72 h in the absence of light. After this time, the solution was dialyzed against distilled water for 2 h using a 3.5 kDa *MWCO* membrane, filtered and lyophilized. All reactions were performed using CP : carrier w/w ratio 5:10. CP-loaded dicarboxy polysaccharides were designated as CP-DCC, CP-DCH, CP-DXA and CP-DXI. The CP release kinetics was investigated using previously employed setup which simulates *in vitro* conditions. (Münster et al., 2019) Term cisplatin (CP) is in the following text also used for released cisplatin residuum, cis-$[Pt(NH_3)_2(H_2O)_2]^{2+}$, to simplify the discussion. Quantitative elemental analysis of CP-carrier conjugates and aliquot samples of released CP was carried out utilizing the energy-dispersive X-ray fluorescence (XRF) spectrometer ARL Quant'X EDXRF Analyzer (Thermo Scientific, USA). The calibration standards used for determining the amount of platinum in the unknown samples were prepared by dissolving a specific amount of CP in PBS of pH 7.4.

2.6 Computational details. Structures of oxidized polysaccharides were prepared *in silico* and optimized at DFT level by using PBE0 functional and standard def-SVP basis set. The PCM solvent model was used to simulate the aqueous environment. The D3 dispersion correction was included to improve the description of weak interactions. Subsequently, CP residues were introduced to suitable –COOH groups and conjugates re-optimized using PBE0 functional and def2-TZVPP basis set with ECP replacing 60 core electrons for platinum and def2-SVP basis set for lighter atoms. This setup was previously optimized for the calculation of structures of platinum complexes. (Pawlak et al., 2014; Vícha et al., 2015)

2.7 Cytotoxicity and in vitro study. As non-tumorigenic cell line, immortalized mouse embryonic fibroblasts NIH/3T3 (ATCC, USA) were used. DMEM was used as a culture medium with addition of 10% FBS, 100 U/mL penicillin and 0.1 mg/mL streptomycin. Further, two tumor cell lines were used in this study: (i) A2780 epithelial ovarian cancer cells and (ii) MCF-7 epithelial-like breast cancer cells established from the pleural effusion from a female suffering from breast adenocarcinoma. Both cell lines were purchased from the European Collection of Authenticated Cell Cultures (ECACC, UK) and were cultivated in RPMI-1640

medium, supplemented with 10% FBS, antibiotics (penicillin 100 U/mL and streptomycin 0.1 mg/mL) and HEPES. The cells were grown in the incubator at 37 °C in a humidified 5% CO_2 mixture with ambient air and subsequently seeded on a 96-well plate at a density ensuring 70% confluence in the day of the treatment. Treatment was performed third day of cultivation, when the culture medium was replaced with a fresh one containing CP-carrier conjugates (concentration 0–500 µM, 200 µL per well). After 24 and 48 h, the cell culture medium with CP-carrier conjugates was removed and the cells were incubated with a fresh medium containing 1 mg/mL of MTT reagent (200 µL per well) for another 4 h. Plates with the cells were wrapped in aluminium foil and kept in a humidified atmosphere at 37 °C. Next, the culture medium with MTT was replaced by DMSO (200 µL per well) to dissolve the formazan crystals, glycine buffer (25 µL per well) was added, gently shaken and the absorbance at 570 nm was recorded using Cytation 3 Imaging reader (BioTek Instruments, USA). The same reader was used in all the biological experiments mentioned further. The IC_{50} values were then calculated by fitting the data with the logistic function to create a sigmoidal dose-response curve. All measurements were performed in tetraplicates.

2.8 Cellular uptake. The A2780 and MCF-7 cells were seeded on a cell culture dishes (25 cm^2) in RPMI-1640 culture medium containing with a standard supplementation and incubated for 48 h. Then, both cell lines were individually treated with 10 µM of platinum compounds (CP, CP-DCC, CP-DCH, CP-DXA, and CP-DXI). This concentration was applied to determine the accumulation of platinum without inducing extensive cell death. After further incubation for 8, 24 and 48 h, the cells were harvested by trypsinization and washed three times with PBS followed by centrifugation (4 °C, 2700 rpm, 7 min) to remove the compounds residues and surface-adsorbed drugs. Cell lysis was carried out mechanically for 2 min in PBS on ice using a micropestle followed by centrifugation (4 °C, 2700 rpm, 7 min). The platinum concentration in the supernatant collected after the centrifugation was determined using the ICP-MS Agilent 7900 (Agilent Technologies, USA). Prepared lysates were diluted 10-fold with MQ water before the analysis, and the Pt concentration was measured by observing the ^{195}Pt isotope. The amount of platinum was expressed in mg/L and then converted to nanograms of Pt per 10^6 cells. The number of cells was counted individually for every single culture dish.

3. Results

3.1 NMR structural study.

Dicarboxylated polysaccharides were prepared by regioselective oxidation of source polysaccharide by sodium periodate, followed by secondary oxidation by chlorite salt, as described in Section *2.2*. Their structure was investigated using a combination of ^1H, ^{13}C NMR spectra and heteronuclear multiplicity-edited ^1H–^{13}C HSQC and ^1H–^{13}C HMBC experiments, (Münster et al., 2017, 2019) see Section *2.4*. ^1H NMR spectra of DCC, DXI, DXA, and DCH are given in Figure 3. Assignment of DCC and DXI signals is based on previous works, (Münster et al., 2019, 2020) spectra of DXA and DCH were solved based on ^1H–^{13}C experiments given in Figures S1 and S2. Full assignment of ^1H and ^{13}C NMR chemical shifts is given in Table S1.

The ^1H NMR spectra clearly illustrate the differences in the structure of individual DCPs. Four relatively narrow signals of DCC confirm simple and well-defined structure of oxidized cellulose chains with *DO* of

98% established based on comparison of intensity of residual signals of non-oxidized units between 3.4-3.6 ppm and signals of oxidized units around 4 ppm. The signals of DXI are somewhat broader, which is likely a result of different conformation of neighboring units discussed in Section *3.4*. Spectra also contain signals of α-(1→6) branched units (about 10% of intensity, marked by # in Figure 3), assigned based on Petersen et al. (Petersen et al., 2015). *DO* was established to be 97 %, similarly to DCC, meaning that combination of α-(1→4) and α-(1→6) bonding in DXI does not hinder periodate nor chlorite oxidation.

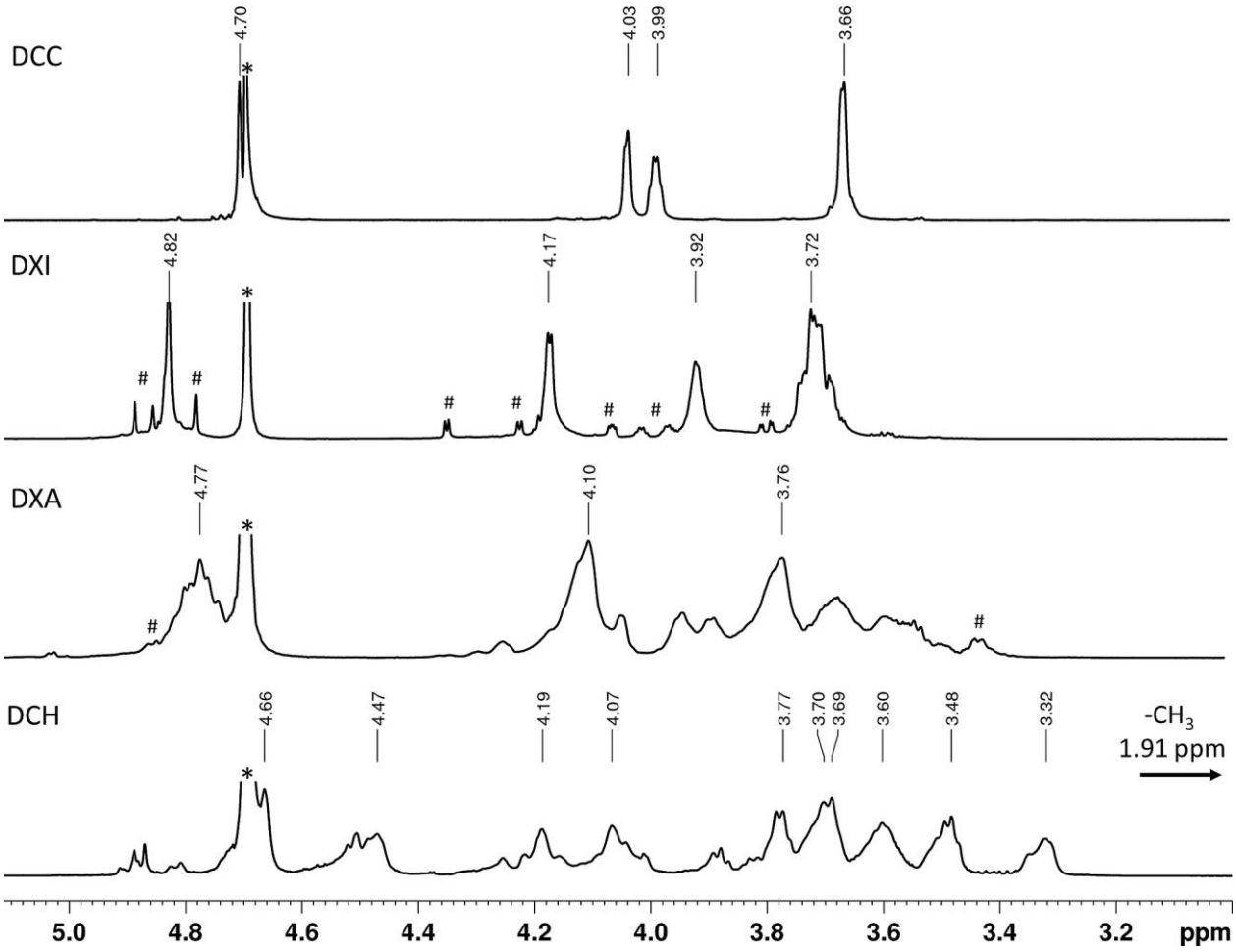

Figure 3 ^{1}H NMR spectra of DCC, DXI, DXA and DCH measured at 298 K in D_2O. Signal of $–CH_3$ group of DCH is not shown for the sake of resolution. The symbol # marks observable signals of branched DXI units and branched non-oxidized units of DXA.

The complex structure of oxidized dextran from *Leuconostoc spp.* is reflected in its ^{1}H spectra featuring five partially-overlapping spin systems (Figure S1). The dominant spin system is composed of only three signals (identified as C1, C5 and C6) and was thus unequivocally assigned to 2,4-DXA (Table S1). The second most intensive one was assigned to 3,4-dicarboxydextran units, based on distinct correlation signal between H1/C1 at 4.75/104.1 ppm and signal at 4.05/72.7 ppm, which was identified as H2/C2, see Table S1. Another two sets of signals have significantly lower intensity, but their chemical shifts are very similar

to those of 2,4-DXA and 3,4-DXA, respectively. They are assumed to belong to respective 2,4-DXA and 3,4-DXA units found in different chemical environment, *i.e.* bound to different neighboring units. The last set of signals, represented e.g. by doublet at 3.44 ppm, was assigned to non-oxidized α-(1→6) and α-(1→3) branched AGUs. Signals of 2,3-DXA units were not identified, which is in agreement with the reported high preference of 3,4-DXA unit formation. (Khomyakov et al., 1965) The total *DO* was established to be ~85 %.

The spectrum of DCH is composed of two spin systems. The pattern of major signals in ^{1}H NMR spectra of DCH is consistent with the expected oxidation of glucuronic unit (GlcA) of HA at positions 2 and 3 and intact N-acetyl-D-glucosamine (NGA) unit, see Table S1 and Figure S2. Note, that position of NGA unit signals in ^{1}H and ^{13}C spectra correspond to those reported for HA derivatives with modified GlcA units. (Wende et al., 2016) The only exception is the signal of C1, which is somewhat more deshielded, likely due to nearby –COOH groups at C3 and C6 of GlcA. The second set of signals has about 30% intensity of major signals and likely belong to intramolecular hemiacetals formed by after the primary oxidation, which were only partially oxidized during the secondary oxidation. Similar behavior was observed for DCC and DXI (Münster et al., 2020). The *DO* of DCH is thus assumed to be ~70% and further optimization of HA oxidation might be required.

3.2 Molecular weight analysis

Results of molecular weight analysis of DCC, DXI, DXA and DCH are summarized in Table 1. The lowest impact of the sequential oxidation on the degree of polymerization *(DP)* of the carrier is observed for dextran (only 4% decrease of *DP* compared to source material). Likely explanation is based on findings of Ishak and Painter (Ishak & Painter, 1978) and Maia et al. (Maia et al., 2011) who described the tendency of periodate-oxidized dextran units to form dense hemiacetal network with neighboring non-oxidized moieties. Network of these relatively stable hemiacetal bonds stabilizes the dextran macromolecules, thus limiting their degradation during secondary oxidation. The two-stage oxidation of cellulose and dextrin resulted in 25–30% decrease of *DP*, which is consistent with previous results. (Münster et al., 2020) Note, that molecular scission of DCC and DXI chains can be either suppressed by using milder reaction conditions (particularly during secondary oxidation) or boosted by the addition of sulfamic acid. (Münster et al., 2020) The most significant decrease of molecular weight is 94% decrease in *DP* between HA and DCH, which was observed despite employed milder conditions, see Section *2.2*. Improvement is definitely possible, but it would require thorough optimization of oxidation procedure.

Table 1 Molecular weight in kDa (M_n – number average, M_w – weight average), polydispersity index (*PDI*), degree of polymerization (*DP*) of the synthesized DCPs, a decrease of *DP* with respect to input polysaccharides (%) and yield of secondary oxidation.

Sample	M_n (kDa)	M_w (kDa)	*PDI* (-)	*DP* (-)	*DP* decrease* (%)	Yield (%)
DCC	42	83	1.95	352	25	97
DXI	23	53	2.33	226	30	96
DXA	45	87	1.92	431	4	89
DCH	13	22	1.67	49	94	98

[*]Calculated as *DP* dicarboxypolysaccharide/*DP* of source polysaccharide × 100 (see Section *2.1*). The *DP* of dicarboxypolysaccharides was calculated with respect to average molar weights of their units, taking into account the degree of oxidation and branching established by NMR (M_{DCC} = 236.1 g/mol, M_{DXI} = 234.4 g/mol, M_{DXA} = 201.8 g/mol and M_{DCH} = 453.1 g/mol).

3.3 Drug loading, characterization of conjugates, and drug release study

Loading of CP to dicarboxypolysaccharides is spontaneous reaction during which chlorido ligands of CP are substituted by carboxylates of the carrier, see Scheme S1 in SI for reaction mechanism. (Münster et al., 2019) Theoretical maximum loading capacity was calculated for each carrier as $M_{CP}/(M_{carrier} \times DO)$ assuming 100% effectivity of reaction between CP and carrier, where M_{CP} is the molar mass of cisplatin, $M_{carrier}$ corresponds to the average molar weight of the basic structural unit established in previous section. The maximum theoretical loading capacity of DCC, DXI and DXA is ~55 wt% of CP in the conjugate, corresponding to about 12.5:10 (CP : carrier) w/w ratio. The presence of intact N-acetyl-D-glucosamine units combined with 70% *DO* reduces maximum loading of DCH to ~33 wt% of CP (5:10) assuming binding of CP only to C2 and C3. If conjugation of CP to –COOH group at C6 of GlcA is also considered, the loading capacity of DCH increases to approx. 45 wt%, (assuming each CP binds two GlcA units).

All carriers were loaded using equal 5:10 (CP : carrier, w/w) reaction ratio, which corresponds to max. 33 wt% of CP in the conjugate, purified and lyophilized, see Section *2.5*. CP loading effectivity was determined by XRF spectroscopy to be 98%, 97%, 90% and 80% for DCC, DXI, DXA and DCH, respectively. Lower loading effectivity of DCH is likely due to higher steric protection of biding sites. Note, however, that this is still considerably higher than loading effectivity reported for unmodified HA. (Cai et al., 2008; Fan et al., 2015) Moreover, despite relatively high amount of loaded CP (27 wt%), no negative impact on the solubility of CP-DCH was observed.

The hydrodynamic radii (d_h) and ζ-potential (ζ) of individual conjugate nano-assemblies formed after dissolution of conjugates were determined by DLS technique, see Table S2 in SI. The d_h of prepared nano-assemblies in water is around 130 nm with exception of CP-DCC conjugate, which is significantly larger (>200 nm). Stronger ionic environment of 0.15M saline solution, which better describe the *in vitro* conditions, led to decrease of domain d_h to ~90 nm for CP-DXI, CP-DXA and CP-DCH and to ~105 nm in the case of CP-DCC. These values are comparable with those reported for other polymeric nanoparticles used in drug-delivery applications. (Haddadi et al., 2016) Such dimensions are also associated with efficient EPR effect. (Haddadi et al., 2016) The ζ-potential values ranging from -58 mV in water to approx. -30 mV in saline indicate good stability of all assemblies in both environments. No particle aggregation was observed.

Next, CP release kinetics from the conjugates was studied. The release of CP requires hydrolysis of COO–Pt bond(s), see Scheme S1 in SI. The rate of reaction is naturally enhanced in environment with high concentration of potential competitive ligands, such as Cl^- or PO_4^{3-}. Hence, to obtain a more reliable results, the release of CP from CP-carrier conjugates was investigated using setup mimicking *in vitro* conditions (PBS, pH 7.4, 37 °C) following earlier works (Münster et al., 2019). The comparison of the cumulative release of CP from individual carriers is given in Figure 4.

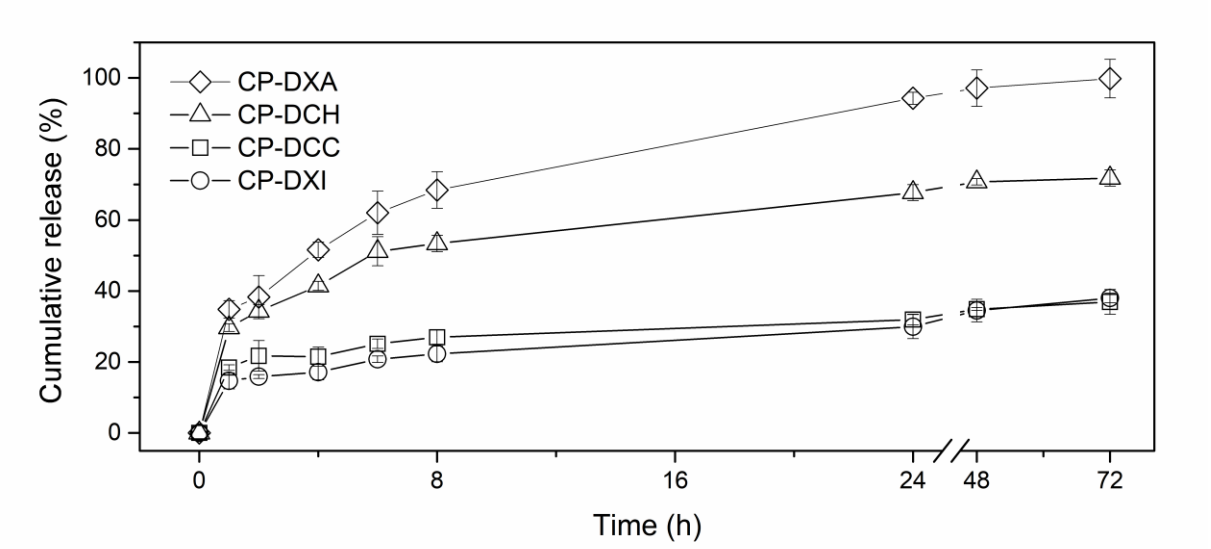

Figure 4 The cumulative release of CP from CP-carrier conjugates throughout 72 h.

Based on previous results, release rates were expected to scale with M_w of the carrier – the smaller the M_w, the faster the release. (Münster et al., 2019) However, structural differences between carriers (partially) overweight the effect of M_w and lead to the emergence of rather unexpected release patterns. For instance, DXA and DCC both have M_w of ~85 kDa (Table 1), which is the highest among tested carriers. Yet, observed relative CP release rates are strikingly different. CP-DXA has the fastest CP release rate (over 95 % of CP released within 24 h), while only 30 % of CP was released from CP-DCC over the same time period. Origin of these differences was rationalized with the aid of DFT calculations, see Section *3.4*.

The second fastest CP release rate (67 % of CP released after 24 h) was observed for CP-DCH and is most likely a result of its low M_w. Note, that observed release rate is similar to CP-DCC derivative with comparable molecular weight, (Münster et al., 2019) suggesting the dominance of bidentate binding in CP-DCH. The slowest release kinetics (29 % of CP released after 24 h) was observed for CP-DXI with M_w of 53 kDa. This is attributed to the branching of DXI in combination with the different conformation of DXI platinum binding sites, as discussed in Section *3.4*.

3.4 DFT structural study

Models of carriers containing six basic structural units (three in case of disaccharide DCH units) were prepared *in silico* from structures of source polysaccharides and optimized on DFT level, see Section *2.6*. CP residues were subsequently introduced to suitable binding sites and structures re-optimized. Structures of carriers are given in Figure 5, for conjugates see Figure S3 in SI. Structures were analyzed with respect to the distance and orientation (conformation) of binding groups and differences in the structure of CP residues.

The repeating β-(1→4) glycosidic bonds in DCC result in the alternating orientation of binding sites. The average distance between closest oxygen atoms of the –COOH group pairs from the same unit (termed O–O distance in the following) is 2.9 ± 0.2 Å, which is similar to distance found in platinum complexes involving carboxylates. (Münster et al., 2019) As a result, no significant deformation of the carrier or cisplatin

structure was found after CP conjugation; the O–O distance remained 2.9 ± 0.2 Å and O–Pt–O angle was 93° ± 2°, close to Cl–Pt–Cl angle in CP optimized at the same level (93°). Absence of significant deformations in the conjugate structure together with lack of larger sidechains that would sterically protect the binding sites (compare DCC and DCH in Figure 6) explains the highest observed CP binding effectivity in CP-DCC (98%, see Section *3.3*).

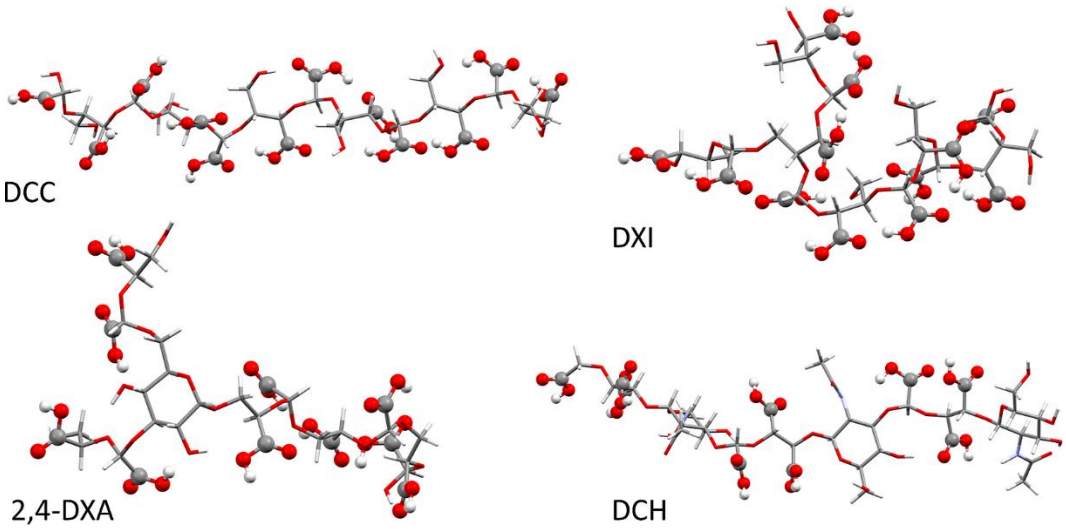

Figure 5 The DFT optimized structures of investigated carriers. Carboxylic groups are emphasized by ball and stick model.

Presence of α-(1→4) glycosidic bonds in DXI should lead to all carboxyl groups being in roughly synperiplanar conformation. DFT calculations, however, revealed that this arrangement is unfavorable due to the repulsion of charged –COOH groups. Every second DXI unit thus adopts antiperiplanar conformation of –COOH groups, which results in repeating structural motif of three synperiplanar and one antiperiplanar –COOH groups, see Figure 5. Two oxidized DXI units may thus effectively bind only one CP residue (O–O distance of synperiplanar units 2.6 ± 0.05 Å), but bidentate binding of the second one would likely require significant conformational changes in DXI structure (O–O distance of antiperiplanar groups >5 Å). This will likely decrease the binding effectivity at higher CP : DXI reaction ratios. On the other hand, the presence of additional negatively charged group in close vicinity of binding site, may, together with comparatively smaller diameter of CP-DXI nano-assemblies (Table S2), explain observed slower initial CP release rates. Essentially, self-assembled conjugate nanoparticles are known to be composed from a "core" formed by more hydrophobic CP residues and the hydrophilic outer shell composed mostly from non-substituted –COO^- groups. (Jeong et al., 2008) Conjugate is then hydrolyzed and positively charged CP residues start to diffuse from the nano-assemblies. Because all investigated carriers are polyanions under physiological pH, CP diffusion rate depends on the diameter of the nano-assembly as well as on its charge density. Branching in CP-DXI leads to the formation of nano-assemblies with smaller diameter than in case of CP-DCC (see Table S2 in SI), but with inherently "denser" negative charge distribution. Hence, the diffusion rate of CP from CP-DXI is initially slower than in case of larger CP-DCC assemblies.

Efficient bidentate binding of CP in combination with high residual negative charge density is also a likely reason for nearly 70 % of CP remaining bonded to both DCC and DXI even after 72 h. In essence, two

molecules of water are required to release a single molecule of CP conjugated by two –COO^- groups. Because core of conjugate nano-assemblies is inherently more hydrophobic than its surface, hydrolysis/release of CP from core area is slowed down. Besides, the released cis-$[Pt(NH_3)_2(H_2O)_2]^{2+}$ complex is held within the nano-assembly by strong electrostatic interactions and may re-attach to abundant –COO^- groups, further slowing the release.

The structure of DCH resembles that of DCC in the alternating orientation of binding sites caused by the presence of β-glycosidic bonds. However, carboxylic groups of DCH are partially screened by sidechains of neighboring non-oxidized NGA units (compare DCC and DCH oxidized units in Figure 6), which is likely responsible for observed lower effectivity of CP conjugation (80%). The oxidation of GlcA units and subsequent repulsion of C2 and C3 carboxylic groups also leads to the opening of former GlcA cycle and C6 carboxylic group being enclosed by sidechains of NGA units (Figure 6). Binding of CP at C6 may thus occur only if these steric barriers are overcome. Hence, bidentate binding of CP at C2 and C3 of DCH is assumed to be a preferred mode of CP conjugation. Note however, that only 30 % of CP remains conjugated to DCH after 72 h. This is assumed to be a result of 2.5-times lower total amount of –COO^- groups in DCH compared to DCC or DXI. Comparatively lower residual negative charge of the DCH particles reduces the strength of electrostatic interactions between CP and the carrier, which thus could diffuse from nano-assemblies more freely. Lower density of –COO^- groups also means lower probability of CP re-attachment to the carrier in comparison with CP-DCC/CP-DXI.

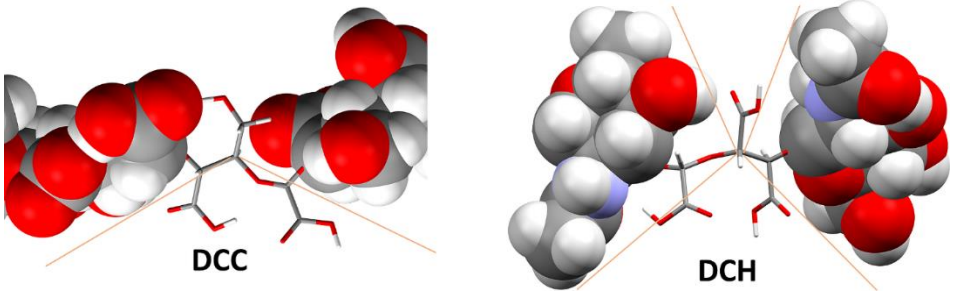

Figure 6 Comparison of CP binding sites in DCC and DCH (stick model). Neighboring units are presented using space-filling model to demonstrate their steric influence. Orange lines are added to better emphasize the availability of each binding site.

With respect to the presence of 2,4- and 3,4-oxidized units in the structure of DXA, two separate structural models were prepared, see Figure 5 for 2,4-DXA structure and Figure S4 in SI for 3,4-DXA. In both cases, oxidation of C4 leads to increased repulsion of carboxylic groups within oxidized unit and an adoption of antiperiplanar conformation of –COOH groups. Carboxyl groups are thus effectively alternating along the DXA chain (O–O distance >5 Å). Bidentate binding of CP to oxidized DXA may still occur due to the relative vicinity of some –COOH groups from neighboring units, *i.e.* CP could bind to C2 and C4' (see CP-DXA in Figure S3), but at the expense of deformations of the carrier structure. The DXA structure thus seems to generally favor the monodentate binding of CP, which readily explains the observed fast drug release rates and also nearly absolute release of bound drug within 72 h. The latter can be also explained by a fact that, contrary to CP-DXI and CP-DCC, only single molecule of water is required to hydrolyze the monodentate bond between CP and DXA. The hydrolysis is thus significantly easier even in the core space of DXA nano-

assemblies. To confirm theoretical predictions, FT-IR spectroscopy was used to investigate the differences in CP binding between the carriers.

3.5 FT-IR platinum binding study

Infrared spectra of free CP, carriers and conjugates were measured and analyzed, see Figures S5–S8. Conjugation of CP to the carriers is accompanied by i) appearance of ν_s NH_3 vibration around 3270 cm^{-1}, ii) asymmetric COO^- vibration band of the carrier around 1604 cm^{-1} by 2–11 cm^{-1}, iii) redshift of COO^- vibration around 1415 cm^{-1} (1381 cm^{-1} in DCH) by 5–9 cm^{-1} and iv) appearance of new band(s) in region between 1300–1400 cm^{-1}. The iv) is of particular interest, because this spectral region is firmly associated with different vibrational modes of carboxylic groups. (Hay & Myneni, 2007) Appearance of new band(s) in this region thus reflect changes in vibrational modes of carboxylic groups upon conjugation with cisplatin. Notably, major differences between DXA and the rest of the carriers are visible in this region. Conjugation of CP to DCC, DXI and DCH leads to increase of intensity of the band between 1300–1320 cm^{-1}, see Figures S5–S7. Because previous heteronuclear NMR analysis (Münster et al., 2019) established bidentate binding mode of CP in CP-DCC, observed changes in FT-IR spectra are assumed to reflect this particular conjugation mode. In CP-DXA spectra, however, another band of comparable intensity appears at 1371 cm^{-1}, see Figure S8. This indicate an alternative, most likely monodentate, CP binding mode in CP-DXA conjugate, which is in agreement with theoretical predictions and other previous findings.

3.6 In vitro cytotoxicity

The cytotoxicity of free carriers (Figure S9, Table 2) and their conjugates with CP (Figure S10, Table 3) was tested against three cell lines; the non-tumor cell line NIH/3T3 and the ovarian and breast cancer cell lines A2780 and MCF-7. The cytotoxicity of carriers and their conjugates was established by MTT assay, see Section *2.7*. With respect to the variations in drug release rates, both 24 and 48 h incubation times were investigated. The presented IC_{50} values are defined as a concentration of compound required to inhibit the cell growth of the particular cell line by 50%. Note, that IC_{50} values of the free carriers are reported in mg/mL, while IC_{50} values of free CP and CP conjugates are in µM and correspond to the total concentration of CP in a culture media (100% release of CP from conjugates is assumed).

Table 2 The IC_{50} (mg/mL) for DCC, DXI, DXA and DCH for non-tumor (NIH/3T3) and tumor (A2780, MCF-7) cell lines for 24 and 48 h incubation time. Values are the average of four independent measurements. Data are displayed as mean ± SD.

Incubation time	**Cell line**	**IC_{50} (mg/mL)**			
		DCC	**DXI**	**DXA**	**DCH**
24 h	**NIH/3T3**	1.21 ± 0.02	1.31 ± 0.02	1.57 ± 0.08	>10
	A2780	1.05 ± 0.11	0.77 ± 0.12	1.13 ± 0.07	>10
	MCF-7	1.19 ± 0.01	1.08 ± 0.04	1.30 ± 0.03	>10
48 h	**NIH/3T3**	1.21 ± 0.02	1.00 ± 0.01	1.30 ± 0.04	>10
	A2780	1.18 ± 0.02	1.08 ± 0.05	1.33 ± 0.07	>10
	MCF-7	0.91 ± 0.01	0.93 ± 0.00	1.06 ± 0.04	>10

The IC_{50} values of DCC, DXI and DXA are between 0.77 mg/mL (DXI, A2780/24 h) and 1.57 mg/mL (DXA, NIH/3T3/24 h) with most of the values between 1.1–1.3 mg/mL. For comprehensive statistical analysis of free carrier results see Figure S11. The DXA shows lower overall cytotoxicity than the other two AGU-based carriers, possibly due to the presence of intact AGU units (lower *DO*). Comparatively, the DCH is the least cytotoxic carrier by far. It shows minimal cytotoxicity for non-tumor NIH/3T3 cells even in at concentration of 10 mg/mL. Also, A2780 and MCF-7 cancer cells evidenced significantly decreased sensitivity towards DCH carrier for both incubation times observed, see Figure S9 in SI.

Overall, all prepared species are suitable as carriers for CP, because their cytotoxicity is negligible at CP therapeutic concentrations. Essentially, effective concentrations of CP are in µg/mL range (*e.g.* IC_{50} of CP for NIH/3T3 after 48h is 5.3 µM, which corresponds to 1.6 µg/mL, M_{CP} = 300 g/mol) while respective IC_{50} values of all carriers are in mg/mL and thus several orders of magnitude larger (*i.e.* less toxic).

The benefits of CP conjugation to the carrier can be deduced from IC_{50} values of corresponding conjugates summarized in Figure 7.

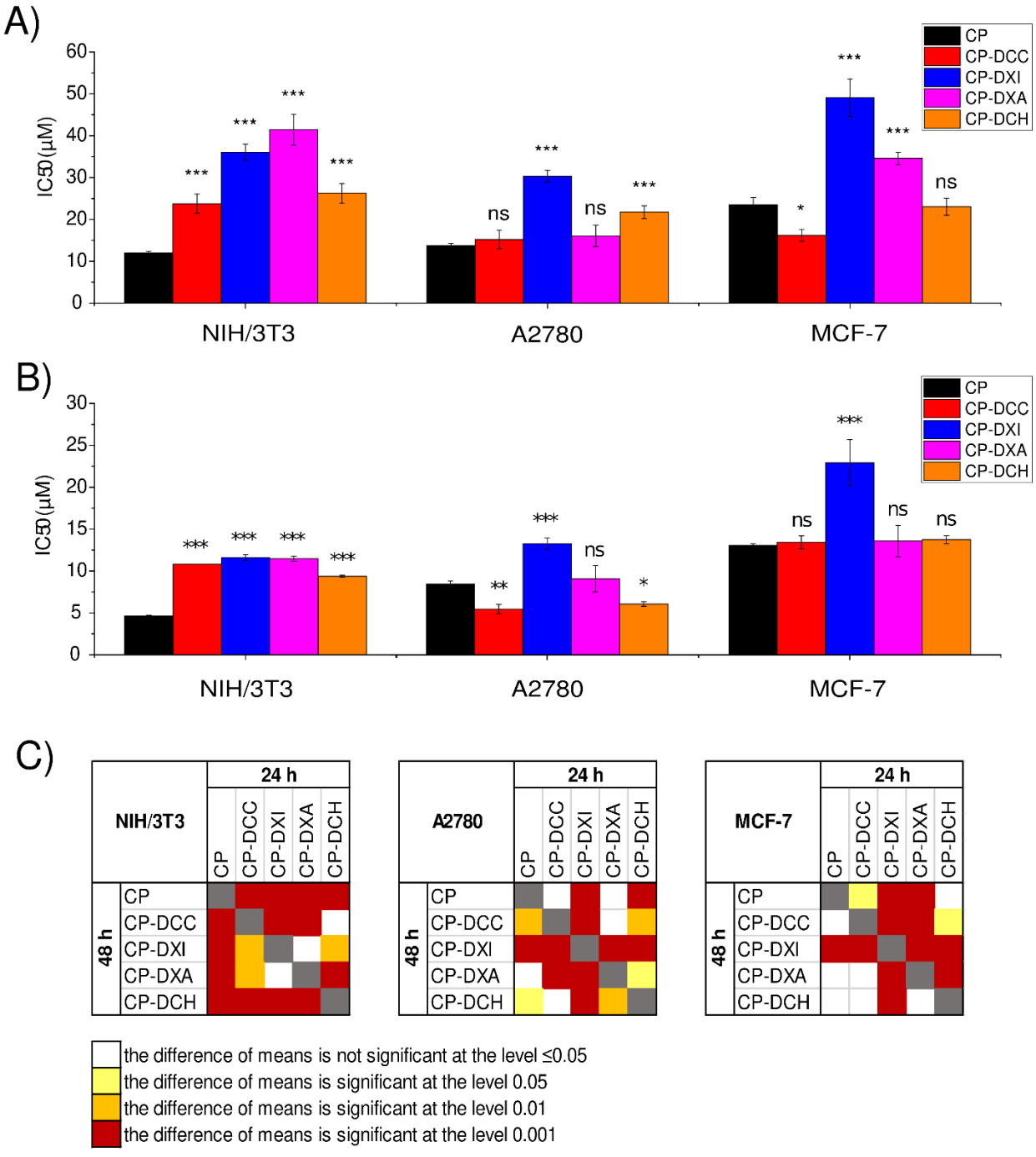

Figure 7 Comparison of IC_{50} values (μM) of polysaccharide CP carriers determined for CP (black), CP-DCC (red), CP-DXI (blue), CP-DXA (pink), and CP-DCH (orange) conjugates after A) 24 h and B) 48 h treatment. Values are the average of four independent measurements. Data are displayed as IC_{50} means ± SD. The IC_{50} values of CP conjugates were related to IC_{50} value of free CP for particular cell line and duration of treatment; ns - not significant, *p<0.05, **p<0.01, ***p<0.001. C) Heat-maps summarizing the statistical significance of differences between IC_{50} means calculated for CP, CP-DCC, CP-DCH, CP-DXA, and CP-DXI in

NIH/3T3, A2780, and MCF-7 cell lines after 24 and 48 h treatments. Statistical analysis was performed using one-way ANOVA followed by Tukey post-hoc test.

All conjugates are significantly less cytotoxic than free CP in the case of non-tumor cell line NIH/3T3 (1.5–3× higher IC_{50}), while mostly having comparable or better cytotoxicity than free CP towards both tumor cell lines. For IC_{50} values and detailed statistical analysis see Table S3 in SI and Figure 7C.

The CP-DCC is the most effective against cancerous cell lines from all tested species, including free CP. Binding of CP to DCC potentiates its cytotoxicity over that of the free drug against both A2780 (after 48 h) and MCF-7 (after 24 h) despite relatively slow CP release rate (only 30% is released after 24 h). The CP-DCH and the CP-DXA are somewhat less cytotoxic towards malignant cell lines than free CP after 24 h of incubation despite fast drug release rates, see Figure 7A. The cytotoxicity of CP-DCH against A2780 cell line significantly improves after 48 h of incubation and is second only to CP-DCC, see Figure 7B, which indicates the potential of DCH in drug delivery applications. Cytotoxicity of CP-DXA also increases after 48 h, when it became comparable to free CP. Rather surprising are poor results of CP-DXI, which is by far the least effective conjugate having IC_{50} towards malignant cell lines approximately twice (1.7–2.2×) larger than free CP. An underlying reason to these observations was revealed by platinum cellular uptake study.

3.7 The cellular uptake of platinum

The A2780 and MCF-7 cell lines were incubated in culture media containing 10μM concentration of free CP or individual CP-loaded carriers for 8, 24 and 48 h, respectively, see Section *2.8* for more details. Results are given in Figure 8, statistical analysis can be found in Figure S12. The highest overall accumulation of Pt was observed in MCF-7 cells after 48 h of incubation. However, MCF-7 cells were assessed to be more than two-times larger than A2780 cells based on automated cell segmentation of quantitative phase images obtained using holographic microscopy (TELIGHT, Czech Republic), see inserts in Figure 8. The average mass of MCF-7 cells is 557.5 pg vs. 240.5 pg for A2780 cells, which explains significantly higher overall amount of accumulated Pt per MCF-7 cell. Therefore, only the qualitative comparison of platinum time-dependent uptake profiles is discussed for different carriers and compared to free CP.

For A2780, the CP-DXA conjugate induced on average the highest Pt accumulation observed across the timepoints (CP-DXA > CP-DCH ≈ CP >> CP-DCC >> CP-DXI). The cellular uptake thus roughly corresponds to the CP release rates (Section *3.3*). In MCF-7, however, the CP-DCH dominates (CP-DCH > CP > CP-DXA > CP-DCC >> CP-DXI). This is likely related to the higher expression of CD44 receptors in MCF-7 cells (Hiscox et al., 2012; Yan et al., 2013, p. 7) compared to A2780 cells, (Piotrowicz et al., 2011) which enhances cellular uptake of CP-DCH.

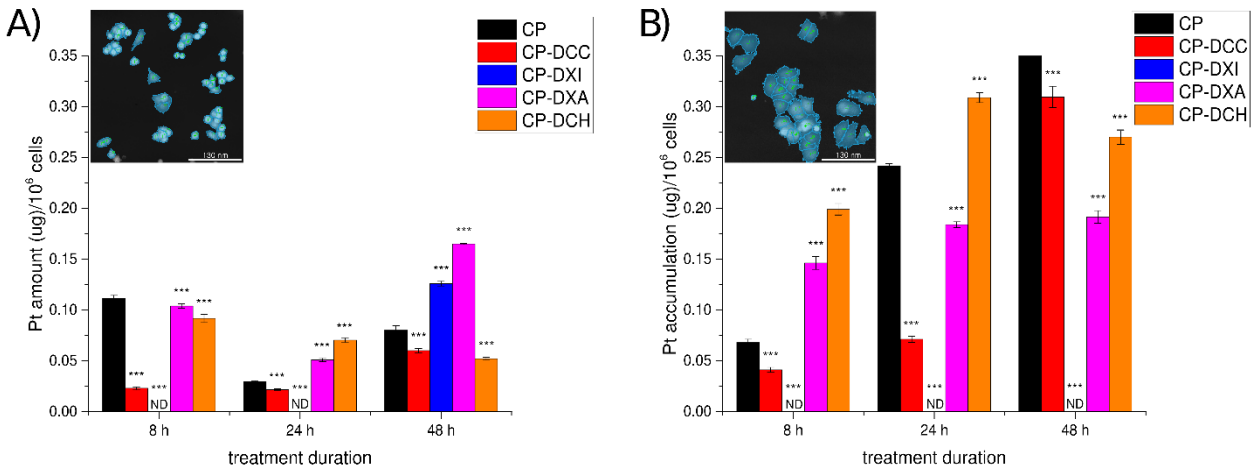

Figure 8 Amount of accumulated Pt in A) A2780 cells and B) MCF-7 cells as a function of incubation time. Inset micrographs illustrate the difference in the cellular dimensions between A2780 and MCF-7, scale bar = 130 µm. The measurements were performed in five repetitions, error bars represent SD. Uptake of individual conjugates was related to that of free CP for particular cell line and incubation time; ns - not significant, *p<0.05, **p<0.01, ***p<0.001. *ND stands for "Not detected".

Interestingly, the cytotoxicity of individual conjugates does not necessary correlate with platinum accumulation. For instance, the amount of platinum accumulated from CP-DCC is in average much lower than in the case of CP-DXA or CP-DCH despite its significantly higher cytotoxicity. Binding of CP to DCC thus increases drug potency in comparison with other carriers, which may be justified *i.e.* by different mode of cellular uptake. This is however not the case for CP-DXI conjugate, which apparently fails to penetrate the cell membrane to significant degree - the amount of platinum accumulated from CP-DXI was below the detection limit of ICP-MS with the exception of A2780/48 h. The reason is unclear, but since CP-DXI has virtually the same *DO*, platinum content and release rates as CP-DCC, we speculate that this might be related to its branched structure and higher negative charge density in CP-DXI discussed in Section *3.4*, which causes larger repulsion with the negatively charged cell membrane.

4. Discussion

Sequential oxidation of different polysaccharides by periodate and chlorite salts is relatively straightforward reaction, but the specific characteristics of source polysaccharides (structure, solubility, crystallinity) has to be considered. Cellulose can be oxidized to DCC from nearly 100% without extensive degradation, however, one has to expect decreased yield and longer oxidation times of primary oxidation due to insolubility of cellulose. Orientation of platinum binding sites in DCC is alternating along the polysaccharide chain due to presence of β-(1→4) bonds between units (see Figure 1). This maximizes their accessibility for conjugation, because it minimizes potential steric clashes between the molecules of conjugating drug. Alternating orientation of binding sites is, together with high *DO* and absence of sidechains, the main reason for the highest observed drug-loading capacity (up to 55 wt%) and conjugation efficacy (98 %) of DCC. Position and orientation of –COOH groups in DCC is also ideal for bidentate binding of CP, which is manifested in relatively slow release of CP from DCC (Section *3.3*). Cytotoxicity of free DCC

is comparable to other AGU-based carriers (DXA, DXI). The CP-DCC conjugates are, however, the most effective against malignant cell lines from all tested combinations, including free CP, despite relatively low accumulation of CP-DCC conjugate in cancer cells and slow drug release rates. Overall, DCC shows excellent qualities as a drug carrier and large potential for further improvement particularly if its cellular uptake can be enhanced.

The dextrin is fully oxidized already after 8 h of primary oxidation due to its partial solubility in water and absence of large crystalline regions. Presence of α-(1→4) bonds and related repulsion of –COOH groups leads to the adoption of alternating syniperiplanar/antiperiplanar conformation of –COOH groups in neighboring oxidized units (Section *3.4*). This has negligible impact on CP binding effectiveness (97 %) at given loading ratio 5:10 (CP : DXI) but may negatively influence the CP binding at higher loading ratios (maximum theoretical loading capacity 55 wt%). Combination of effective bidentate binding of CP and branching of DXI has a significant impact on its drug-delivery characteristics because it slows down the initial drug release rates, likely contribute to the poor internalization of the carried drug by the cancer cells and thus decrease the conjugate cytotoxicity. DXI thus cannot be recommended as a carrier for CP.

Primary oxidation of dextran is finished in 4 h and does not lead to any significant degradation of the DXA chain, probably due to the formation of stabilizing hemiacetal bonds between neighboring units. (Maia et al., 2011) DXA has a relatively complex structure composed of α-(1→6) bonded 2,4- and 3,4-oxidized units and non-oxidized α-(1→3) branching units. The presence of the latter limits the maximum *DO* of DXA to ~85%, while the DXA loading capacity (>55 wt%) and CP-binding effectivity (90%) are comparable to those of DCC and DXI. However, alternating direction of –COOH groups along the DXA backbone most likely results in prevalent monodentate binding of CP, which explains rather fast drug release rates. This brings up a question whether the CP-DXA conjugate would be sufficiently stable *in vivo* to accumulate in tumor or the drug would be released prematurely in blood stream. High molecular weight derivatives or various nanoformulations might be potentially used to counter this issue. On the other hand, CP-DXA conjugate has lowest cytotoxicity towards non-tumor NIH/3T3 cells (about 50% less cytotoxic than CP-DCC, nearly 3-times less cytotoxic than free CP), while having similar effectivity as free CP against A2780 cell line, which makes it potentially interesting for drug-delivery applications.

Unique structure of DCH brings both advantages and drawbacks when compared to AGU-based carriers. Some disadvantages of DCH, such as high degradation of HA chains during the oxidation (over 90% loss of *DP*), relatively low degree of oxidation (70%) and lower drug binding effectiveness (80%) may be improved by further optimization of oxidation reaction conditions and/or loading protocol. On the other hand, lower maximum loading capacity in comparison with AGU-based derivatives (33 wt%) is given by the resistance of N-acetyl-D-glucosamine units to periodate oxidation. Nevertheless, oxidation of HA to DCH still essentially triples the number of carboxylic groups available, improves loading efficiency and reduces the risk of undesirable crosslinking reactions during loading when compared to HA. CP release rate from CP-DCH is comparable to the CP-DCC of similar molecular weight, which indicates the dominance of bidentate binding of the drug further confirmed by FT-IR study. The largest advantage of DCH lies in its biological properties. The cytotoxicity of free DCH is several times lower in comparison to AGU-based carriers, while the cytotoxicity of CP-DCH conjugates is comparable or better than that of free CP towards malignant cells. Moreover, the higher expression of CD44 receptors in MCF-7 cell line presumably increased cellular uptake

of CP-DCH. The DCH thus has a large potential for further development, however, additional studies are needed.

5. Conclusions

The structure of source polysaccharide was found to have important, sometimes even crucial, impact on drug-delivery and *in vitro* biological properties of CP-carrier conjugates. Following observations regarding the relationship between the structure of the polysaccharides and their drug-delivery characteristics were derived:

i) While the drug loading capacity of the carrier depends on the density of –COOH groups in its structure (the higher, the better), the drug loading effectivity is affected by the conformation of binding sites, which determines the mode of binding (bidentate vs. monodentate), and by their steric protection (the less, the better).

ii) The mode of drug binding is the main force influencing the drug release kinetics (monodentate binding = faster release), followed by the molecular weight of the carrier (the lower the weight, the faster the release) and branching, which presence reduces the initial drug release rate.

iii) The cytotoxicity of free carriers is largely dictated by the composition of their basic structural units (all AGU-based carriers were considerably more cytotoxic than HA-based carrier) and is further influenced by the amount of modified basic structural units (degree of oxidation) while impact of branching is limited.

iv) The cytotoxicity of the CP-carrier conjugates is higher for linear carriers (CP-DCC, CP-DCH) and is reduced for branched carriers, particularly in combination with bidentate binding of CP (CP-DXI).

v) The cellular uptake of platinum roughly correlates with the drug release kinetics and is thus likely influenced by the same factors. It can be however enhanced further by biological targeting (CP-DCH) or thwarted by unfavorable combination of structural aspects (CP-DXI). Notably, the cytotoxicity of the CP-carrier conjugates does not (always) correlate with the amount of platinum accumulated within the cells (CP-DCC), possibly due to different cellular uptake pathways, *i.e.* passive diffusion vs. active transport.

To summarize, polysaccharides with β-(1→4) glycosidic bonds, vicinal –OH groups at C2 and C3 and linear structure (cellulose, HA) seem to possess the best combination of structural features and properties for drug delivery applications, making them particularly promising for further studies.

Acknowledgements

This work was supported by the Ministry of Education, Youth and Sports of the Czech Republic – DKRVO (RP/CPS/2020/006). M. Fojtů and M. Masařík were supported by the project Advanced Functional Nanorobots reg. No. CZ.02.1.01/0.0/0.0/15_003/0000444. M. Muchová was supported by the internal grant for specific research from TBU in Zlin no. IGA/CPS/2020/003. M. Fojtů was further supported by funds from the Faculty of Medicine MU Brno to junior researcher. CIISB research infrastructure project LM2018127 funded by Ministry of Education, Youth and Sports of the Czech Republic is acknowledged for the financial support of the NMR measurements at the Josef Dadok CEITEC core facility in Brno. Computational resources were supplied by the project "e-Infrastruktura CZ" (e-INFRA LM2018140) provided within the program Projects of Large Research, Development and Innovations Infrastructures.

Associated Information

*Supplementary Information*is available - 2D NMR spectra of DXA and DCH, DFT optimized structures and FT-IR spectra of conjugates and carriers, DLS results, relative cell viabilities with respect to the carriers/drug concentration and cell line, statistical evaluation of biological results.

Author Information

Author Contributions. L. Münster – synthesis and characterization of carriers and conjugates, M. Fojtů – *in vitro* tests, cellular uptake, statistical analysis. Z. Capáková *in vitro* tests on non-tumor cell line, M. Muchová – drug release studies, L. Musilová – contributed to synthesis of carriers, T. Vaculovič – ICP/MS studies, J. Balvan – contributed to cellular uptake studies. I. Kuřitka – writing of the manuscript, experimental design, M. Masařík – design of *in vitro* studies, J. Vícha - synthesis of cisplatin and conjugates, experimental design, NMR analysis, DFT calculations, writing of the manuscript.

Notes

The authors declare no competing financial interest.

References:

Assmann, V., Fieber, C., Herrlich, P., Hofmann, M., Termeer, C. C., Ahrens, T., & Simon, J. C. (2001). CD44 is the Principal Mediator of Hyaluronic-Acid-Induced Melanoma Cell Proliferation. *Journal of Investigative Dermatology*, *116*(1), 93–101. https://doi.org/10.1046/j.1523-1747.2001.00236.x

Babjaková, E., Branná, P., Kuczyńska, M., Rouchal, M., Prucková, Z., Dastychová, L., Vícha, J., & Vícha, R. (2016). *An adamantane-based disubstituted binding motif with picomolar dissociation constants for cucurbit[n]urils in water and related quaternary assemblies*. *6*(107), 105146–105153. https://doi.org/10.1039/C6RA23524G

Borland, G., Ross, J. A., & Guy, K. (1998). Forms and functions of CD44. *Immunology*, *93*(2), 139–148.

Cai, S., Xie, Y., Bagby, T. R., Cohen, M. S., & Forrest, M. L. (2008). Intralymphatic Chemotherapy Using a Hyaluronan–Cisplatin Conjugate. *Journal of Surgical Research*, *147*(2), 247–252. https://doi.org/10.1016/j.jss.2008.02.048

Fan, X., Zhao, X., Qu, X., & Fang, J. (2015). PH sensitive polymeric complex of cisplatin with hyaluronic acid exhibits tumor-targeted delivery and improved in vivo antitumor effect. *International Journal of Pharmaceutics*, *496*(2), 644–653. https://doi.org/10.1016/j.ijpharm.2015.10.066

Fraser, J. R. E., Laurent, T. C., & Laurent, U. B. G. (1997). Hyaluronan: Its nature, distribution, functions and turnover. *Journal of Internal Medicine*, *242*(1), 27–33. https://doi.org/10.1046/j.1365-2796.1997.00170.x

Goodarzi, N., Varshochian, R., Kamalinia, G., Atyabi, F., & Dinarvand, R. (2013). A review of polysaccharide cytotoxic drug conjugates for cancer therapy. *Carbohydrate Polymers*, *92*(2), 1280–1293. https://doi.org/10.1016/j.carbpol.2012.10.036

Goodison, S., Urquidi, V., & Tarin, D. (1999). CD44 cell adhesion molecules. *Molecular Pathology: MP*, *52*(4), 189–196. https://doi.org/10.1136/mp.52.4.189

Haddadi, A., Jahan, S. T., & Sadat, S. M. A. (2016). Effects of Size and Surface Charge of Polymeric Nanoparticles on in Vitro and in Vivo Applications. *Journal of Biomaterials and Nanobiotechnology*, *7*(2), 720–726. https://doi.org/10.4236/jbnb.2016.72011

Hay, M. B., & Myneni, S. C. B. (2007). Structural environments of carboxyl groups in natural organic molecules from terrestrial systems. Part 1: Infrared spectroscopy. *Geochimica et Cosmochimica Acta*, *71*(14), 3518–3532. https://doi.org/10.1016/j.gca.2007.03.038

Hiscox, S., Baruha, B., Smith, C., Bellerby, R., Goddard, L., Jordan, N., Poghosyan, Z., Nicholson, R. I., Barrett-Lee, P., & Gee, J. (2012). Overexpression of CD44 accompanies acquired tamoxifen resistance in MCF7 cells and augments their sensitivity to the stromal factors, heregulin and hyaluronan. *BMC Cancer*, *12*, 458. https://doi.org/10.1186/1471-2407-12-458

Huang, G., Mei, X., Xiao, F., Chen, X., Tang, Q., & Peng, D. (2015). Applications of Important Polysaccharides in Drug Delivery. *Current Pharmaceutical Design*, *21*(25), 3692–3696.

Ishak, M. F., & Painter, T. J. (1978). Kinetic evidence for hemiacetal formation during the oxidation of dextran in aqueous periodate. *Carbohydrate Research*, *64*, 189–197. https://doi.org/10.1016/S0008-6215(00)83700-3

Jeong, Y.-I., Kim, S.-T., Jin, S.-G., Ryu, H.-H., Jin, Y.-H., Jung, T.-Y., Kim, I.-Y., & Jung, S. (2008). Cisplatin-incorporated hyaluronic acid nanoparticles based on ion-complex formation. *Journal of Pharmaceutical Sciences*, *97*(3), 1268–1276. https://doi.org/10.1002/jps.21103

Johnstone, T. C., Suntharalingam, K., & Lippard, S. J. (2016). The Next Generation of Platinum Drugs: Targeted Pt(II) Agents, Nanoparticle Delivery, and Pt(IV) Prodrugs. *Chemical Reviews*, *116*(5), 3436–3486. https://doi.org/10.1021/acs.chemrev.5b00597

Khomyakov, K. P., Penenzhik, M. A., Virnik, A. D., & Rogovin, Z. A. (1965). Synthesis of dialdehydo- and dicarboxydextran. *Polymer Science U.S.S.R.*, *7*(6), 1140–1145. https://doi.org/10.1016/0032-3950(65)90394-1

706 Kristiansen, K. A., Potthast, A., & Christensen, B. E. (2010). Periodate oxidation of polysaccharides for
707 modification of chemical and physical properties. *Carbohydrate Research*, *345*(10), 1264–1271.
708 https://doi.org/10.1016/j.carres.2010.02.011
709 Maekawa, E., & Koshijima, T. (1984). Properties of 2,3-dicarboxy cellulose combined with various
710 metallic ions. *Journal of Applied Polymer Science*, *29*(7), 2289–2297.
711 https://doi.org/10.1002/app.1984.070290705
712 Maia, J., Carvalho, R. A., Coelho, J. F. J., Simões, P. N., & Gil, M. H. (2011). Insight on the periodate
713 oxidation of dextran and its structural vicissitudes. *Polymer*, *52*(2), 258–265.
714 https://doi.org/10.1016/j.polymer.2010.11.058
715 Mehvar, R. (2000). Dextrans for targeted and sustained delivery of therapeutic and imaging agents.
716 *Journal of Controlled Release*, *69*(1), 1–25. https://doi.org/10.1016/S0168-3659(00)00302-3
717 Miao, T., Wang, J., Zeng, Y., Liu, G., & Chen, X. (2018). Polysaccharide-Based Controlled Release Systems
718 for Therapeutics Delivery and Tissue Engineering: From Bench to Bedside. *Advanced Science*,
719 *5*(4), 1700513. https://doi.org/10.1002/advs.201700513
720 Münster, L., Fojtů, M., Capáková, Z., Vaculovič, T., Tvrdoňová, M., Kuřitka, I., Masařík, M., & Vícha, J.
721 (2019). Selectively oxidized cellulose with adjustable molecular weight for controlled release of
722 platinum anticancer drugs. *Biomacromolecules*, *20*(4), 1623–1634.
723 https://doi.org/10.1021/acs.biomac.8b01807
724 Münster, L., Hanulíková, B., Machovský, M., Latečka, F., Kuřitka, I., & Vícha, J. (2020). Mechanism of
725 sulfonation-induced chain scission of selectively oxidized polysaccharides. *Carbohydrate*
726 *Polymers*, *229*, 115503. https://doi.org/10.1016/j.carbpol.2019.115503
727 Münster, L., Vícha, J., Klofáč, J., Masař, M., Hurajová, A., & Kuřitka, I. (2018). Dialdehyde Cellulose
728 Crosslinked Poly(vinyl alcohol) Hydrogels: Influence of Catalyst and Crosslinker Shelf Life.
729 *Carbohydrate Polymers*, *198*, 181–190. https://doi.org/10.1016/j.carbpol.2018.06.035

730 Münster, L., Vícha, J., Klofáč, J., Masař, M., Kucharczyk, P., & Kuřitka, I. (2017). Stability and aging of
731 solubilized dialdehyde cellulose. *Cellulose*, *24*(7), 2753–2766. https://doi.org/10.1007/s10570-
732 017-1314-x
733 Ohta, S., Hiramoto, S., Amano, Y., Sato, M., Suzuki, Y., Shinohara, M., Emoto, S., Yamaguchi, H., Ishigami,
734 H., Sakai, Y., Kitayama, J., & Ito, T. (2016). Production of Cisplatin-Incorporating Hyaluronan
735 Nanogels via Chelating Ligand–Metal Coordination. *Bioconjugate Chemistry*, *27*(3), 504–508.
736 https://doi.org/10.1021/acs.bioconjchem.5b00674
737 Ohya, Y., Masunaga, T., Baba, T., & Ouchi, T. (1996). Synthesis and cytotoxic activity of dextran carrying
738 cis-dichloro(cyclohexane-trans-l-1,2-diamine)platinum(II) complex. *Journal of Biomaterials*
739 *Science, Polymer Edition*, *7*(12), 1085–1096. https://doi.org/10.1163/156856296X00570
740 Pawlak, T., Niedzielska, D., Vícha, J., Marek, R., & Pazderski, L. (2014). Dimeric Pd(II) and Pt(II) chloride
741 organometallics with 2-phenylpyridine and their solvolysis in dimethylsulfoxide. *Journal of*
742 *Organometallic Chemistry*, *759*, 58–66. https://doi.org/10.1016/j.jorganchem.2014.02.016
743 Petersen, B. O., Motawie, M. S., Møller, B. L., Hindsgaul, O., & Meier, S. (2015). NMR characterization of
744 chemically synthesized branched α-dextrin model compounds. *Carbohydrate Research*, *403*,
745 149–156. https://doi.org/10.1016/j.carres.2014.05.011
746 Piotrowicz, R. S., Damaj, B. B., Hachicha, M., Incardona, F., Howell, S. B., & Finlayson, M. (2011). A6
747 Peptide Activates CD44 Adhesive Activity, Induces FAK and MEK Phosphorylation, and Inhibits
748 the Migration and Metastasis of CD44-Expressing Cells. *Molecular Cancer Therapeutics*, *10*(11),
749 2072–2082. https://doi.org/10.1158/1535-7163.MCT-11-0351
750 Quan, Y. H., Kim, B., Park, J.-H., Choi, Y., Choi, Y. H., & Kim, H. K. (2014). Highly sensitive and selective
751 anticancer effect by conjugated HA-cisplatin in non-small cell lung cancer overexpressed with
752 CD44. *Experimental Lung Research*, *40*(10), 475–484.
753 https://doi.org/10.3109/01902148.2014.905656

754 Raudenska, M., Balvan, J., Fojtu, M., Gumulec, J., & Masarik, M. (2019). Unexpected therapeutic effects
755 of cisplatin. *Metallomics*, *11*(7), 1182–1199. https://doi.org/10.1039/C9MT00049F
756 Sarwat, F., Qader, S. A. U., Aman, A., & Ahmed, N. (2008). Production & Characterization of a Unique
757 Dextran from an Indigenous Leuconostoc mesenteroides CMG713. *International Journal of*
758 *Biological Sciences*, *4*(6), 379–386.
759 Schanté, C. E., Zuber, G., Herlin, C., & Vandamme, T. F. (2011). Chemical modifications of hyaluronic acid
760 for the synthesis of derivatives for a broad range of biomedical applications. *Carbohydrate*
761 *Polymers*, *85*(3), 469–489. https://doi.org/10.1016/j.carbpol.2011.03.019
762 Schlechter, B., Neumann, A., Wilchek, M., & Arnon, R. (1989). Soluble polymers as carriers of cis-
763 platinum. *Journal of Controlled Release*, *10*(1), 75–87. https://doi.org/10.1016/0168-
764 3659(89)90019-9
765 Shi, Y., & Dabrowiak, J. C. (2012). Host –guest interactions involving platinum anticancer agents. DNA
766 binding and cytotoxicity of a β-cyclodextrin-adamantane-Pt(IV) complex. *Inorganica Chimica*
767 *Acta*, *393*, 337–339. https://doi.org/10.1016/j.ica.2012.06.021
768 Sirviö, J. A., Liimatainen, H., Visanko, M., & Niinimäki, J. (2014). Optimization of dicarboxylic acid
769 cellulose synthesis: Reaction stoichiometry and role of hypochlorite scavengers. *Carbohydrate*
770 *Polymers*, *114*, 73–77. https://doi.org/10.1016/j.carbpol.2014.07.081
771 Varshosaz, J. (2012). Dextran conjugates in drug delivery. *Expert Opinion on Drug Delivery*, *9*(5), 509–523.
772 https://doi.org/10.1517/17425247.2012.673580
773 Vícha, J., Novotný, J., Straka, M., Repisky, M., Ruud, K., Komorovsky, S., & Marek, R. (2015). Structure,
774 solvent, and relativistic effects on the NMR chemical shifts in square-planar transition-metal
775 complexes: Assessment of DFT approaches. *Physical Chemistry Chemical Physics*, *17*(38), 24944–
776 24955. https://doi.org/10.1039/C5CP04214C

Wang, X., & Guo, Z. (2012). Targeting and delivery of platinum-based anticancer drugs. *Chemical Society Reviews*, *42*(1), 202–224. https://doi.org/10.1039/C2CS35259A

Wende, F. J., Gohil, S., Mojarradi, H., Gerfaud, T., Nord, L. I., Karlsson, A., Boiteau, J.-G., Kenne, A. H., & Sandström, C. (2016). Determination of substitution positions in hyaluronic acid hydrogels using NMR and MS based methods. *Carbohydrate Polymers*, *136*, 1348–1357. https://doi.org/10.1016/j.carbpol.2015.09.112

Wilson, J. J., & Lippard, S. J. (2014). Synthetic Methods for the Preparation of Platinum Anticancer Complexes. *Chemical Reviews*, *114*(8), 4470–4495. https://doi.org/10.1021/cr4004314

Yan, W., Chen, Y., Yao, Y., Zhang, H., & Wang, T. (2013). Increased invasion and tumorigenicity capacity of CD44+/CD24- breast cancer MCF7 cells in vitro and in nude mice. *Cancer Cell International*, *13*, 62. https://doi.org/10.1186/1475-2867-13-62

Graphical abstract: